LETTER

https://doi.org/10.1038/s41586-018-0319-4

Resistance-gene-directed discovery of a natural-product herbicide with a new mode of action

Yan Yan[1,8], Qikun Liu[2,8], Xin Zang[3,4,8], Shuguang Yuan[5], Undramaa Bat-Erdene[1], Calvin Nguyen[2], Jianhua Gan[6], Jiahai Zhou[3,4]*, Steven E. Jacobsen[2]* & Yi Tang[1,7]*

Bioactive natural products have evolved to inhibit specific cellular targets and have served as lead molecules for health and agricultural applications for the past century[1–3]. The post-genomics era has brought a renaissance in the discovery of natural products using synthetic-biology tools[4–6]. However, compared to traditional bioactivity-guided approaches, genome mining of natural products with specific and potent biological activities remains challenging[4]. Here we present the discovery and validation of a potent herbicide that targets a critical metabolic enzyme that is required for plant survival. Our approach is based on the co-clustering of a self-resistance gene in the natural-product biosynthesis gene cluster[7–9], which provides insight into the potential biological activity of the encoded compound. We targeted dihydroxy-acid dehydratase in the branched-chain amino acid biosynthetic pathway in plants; the last step in this pathway is often targeted for herbicide development[10]. We show that the fungal sesquiterpenoid aspterric acid, which was discovered using the method described above, is a sub-micromolar inhibitor of dihydroxy-acid dehydratase that is effective as a herbicide in spray applications. The self-resistance gene *astD* was validated to be insensitive to aspterric acid and was deployed as a transgene in the establishment of plants that are resistant to aspterric acid. This herbicide-resistance gene combination complements the urgent ongoing efforts to overcome weed resistance[11]. Our discovery demonstrates the potential of using a resistance-gene-directed approach in the discovery of bioactive natural products.

Weeds are a major source of crop losses, and the evolution of herbicide resistance in weeds has led to an urgent need for new herbicides with novel modes of action[11–14]. The branched-chain amino acid (BCAA) biosynthetic pathway is essential for plant growth[10]. It is not present in animals and is therefore a validated target for highly specific weed-control agents[10]. The BCAA biosynthetic pathway in plants is carried out by three enzymes: acetolactate synthase (ALS), acetohydroxy acid isomeroreductase (KARI), and dihydroxyacid dehydratase (DHAD) (Fig. 1a). Given the success of targeting ALS for herbicide development[11], it is notable that no herbicide that targets either of the other two enzymes has been developed. DHAD is an essential and highly conserved enzyme among plant species that catalyses β-dehydration reactions to yield α-keto acid precursors to isoleucine, valine and leucine[15,16] (Extended Data Fig. 1a, Supplementary Fig. 1). Efforts towards synthetic DHAD inhibitors resulted in compounds with submicromolar inhibition constants (K_i), however, the compounds have no reported *in planta* activity[17] (Extended Data Fig. 1b).

Filamentous fungi are prolific producers of natural products, many of which have biological activities that aid the fungi in colonizing and killing plants[1,2,18]. Therefore, fungal natural products represent a promising source of potential leads for herbicides. The abundance of sequenced fungal genomes enables genome mining of new natural products with novel biological activities[4,6]. Although no natural-product inhibitors of DHAD are known to date, we reason that a fungal natural product with this property might exist, given the indispensable role of BCAA biosynthesis in plants[10].

To identify natural-product biosynthetic gene clusters that may encode a DHAD inhibitor, we hypothesized that such a cluster must contain an additional copy of DHAD that is insensitive to the inhibitor, thereby providing the required self-resistance for the producing organism to survive. Genes encoding a self-resistance enzyme are frequently found in microbial natural-product gene clusters, as highlighted by the presence of an insensitive copy of HMG-CoA reductase (HMGR) and inosine monophosphate dehydrogenase (IMPDH) in the gene clusters of lovastatin (that targets HMGR) and mycophenolic acid (that targets IMPDH), respectively[19,20] (Extended Data Fig. 1c). This phenomenon has been used to predict molecular targets of natural products, as well as to identify gene clusters of natural products of known activities[5,7,9].

To identify possible self-resistance enzymes, we scanned sequenced fungal genomes to search for co-localization of genes encoding DHAD with core biosynthetic enzymes, such as terpene cyclases and polyketide synthases among others[21,22]. We identified a well-conserved set of four genes across multiple fungal genomes (Fig. 1b), including the common soil fungus *Aspergillus terreus* that is best known for producing lovastatin. The conserved gene clusters include genes that encode a sesquiterpene cyclase homologue (*astA*), two cytochrome P450 genes (*astB* and *astC*) and a homologue of DHAD (*astD*). Genes outside of this cluster are not conserved across the identified genomes and are hence unlikely to be involved in the biosynthesis of natural products. AstD is the second copy of DHAD encoded in the genome, and is approximately 70% similar to the housekeeping copy that is well-conserved across fungi (Supplementary Fig. 2). Therefore, AstD is potentially a self-resistance enzyme that confers resistance to the encoded natural product. As with a majority of biosynthetic gene clusters in sequenced fungal genomes, the *ast* cluster has not been associated with the production of a known natural product[4].

To identify the natural product encoded by the *ast* cluster, we heterologously expressed *astA*, *astB* and *astC* genes in the host *Saccharomyces cerevisiae* RC01[23]. New compounds that emerged were purified and their structures were elucidated using NMR spectroscopy (Supplementary Fig. 3, Supplementary Table 5). RC01 cells expressing only *astA* produced a new sesquiterpene (**1**), which was confirmed to be (−)-daucane (Supplementary Fig. 4). RC01 cells expressing both *astA* and *astB* led to the biosynthesis of a new product that was determined structurally to be the α-epoxy carboxylate (**2**) (Fig. 1c). When *astA*, *astB* and *astC* were expressed together, a new compound (**3**) became the dominant product (approximately 20 mg l^{-1}). Full structural determination revealed **3** to be the tricyclic aspteric acid, which is a previously isolated compound[24] (Fig. 1c). The biosynthetic pathway for aspteric

[1]Department of Chemical and Biomolecular Engineering, University of California Los Angeles, Los Angeles, CA, USA. [2]Department of Molecular, Cell, and Developmental Biology and Howard Hughes Medical Institute, University of California Los Angeles, Los Angeles, CA, USA. [3]State Key Laboratory of Bio-organic and Natural Products Chemistry, Center for Excellence in Molecular Synthesis, Shanghai Institute of Organic Chemistry, Chinese Academy of Sciences, Shanghai, China. [4]Department of Chemistry, Shanghai Normal University, Shanghai, China. [5]Laboratory of Physical Chemistry of Polymers and Membranes, Ecole Polytechnique Fédérale de Lausanne, Lausanne, Switzerland. [6]State Key Laboratory of Genetic Engineering, Collaborative Innovation Center of Genetics and Development, Department of Physiology and Biophysics, School of Life Sciences, Fudan University, Shanghai, China. [7]Department of Chemistry and Biochemistry, University of California Los Angeles, Los Angeles, CA, USA. [8]These authors contributed equally: Yan Yan, Qikun Liu, Xin Zang. *e-mail: jiahai@mail.sioc.ac.cn; jacobsen@ucla.edu; yitang@ucla.edu

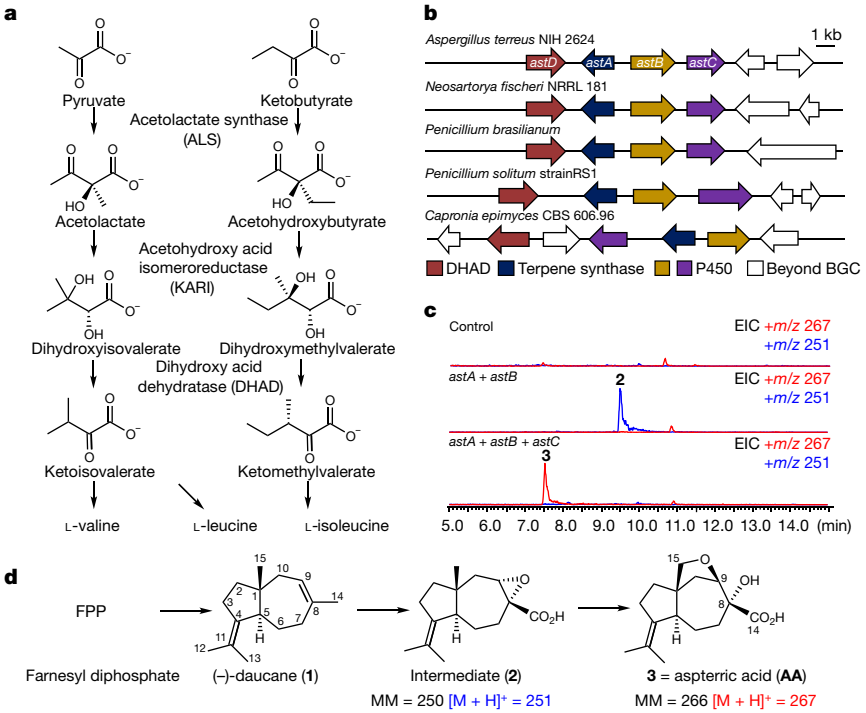

Fig. 1 | Genome mining of a DHAD inhibitor and biosynthesis of aspterric acid. a, Valine, leucine and isoleucine are produced by two parallel pathways using three enzymatic steps: ALS, KARI and DHAD. **b**, A 17-kb biosynthetic gene cluster (BGC) from *A. terreus* containing four open reading frames (ORFs), which are also conserved among several fungal species. *astA* has sequence homology to sesquiterpene cyclase; *astB* and *astC* are predicted to be P450 monooxygenases; *astD* is predicted to encode a DHAD and is proposed to confer self-resistance in the presence of the natural product produced in the cluster. **c**, High-performance liquid chromatography–mass spectrometry (HPLC–MS) traces of metabolites produced from *S. cerevisiae* RC01 expressing the different *ast* genes under the P_{ADH2} promoter control. Control, *S. cerevisiae* without expression plasmids; *S. cerevisiae* transformed with plasmids expressing *astA* and *astB*, which produces **2**; and *S. cerevisiae* transformed with plasmids expressing *astA*–*C*, which produces aspterric acid at a titre of 20 mg l^{-1}. The experiments were repeated independently with similar results three times. EIC, extracted ion chromatogram. **d**, Proposed biosynthetic pathway of aspterric acid. AstA cyclizes farnesyl diphosphate (FPP) into **1** and the P450 enzymes AstB and AstC then sequentially transform **1** into **2** and aspterric acid (**3**, AA), respectively. MM, molecular mass.

acid is therefore concise: after cyclization of farnesyl diphosphate by AstA to create the carbon skeleton in **1**, AstB catalyses oxidation of **1** to yield the epoxide **2**. Further oxidation by AstC at carbon 15 yields an alcohol, which can undergo intramolecular epoxide opening to create aspterric acid (Fig. 1d).

Upon its initial discovery, aspterric acid was shown to have inhibitory activity towards *Arabidopsis thaliana*, however, the mode of action was not known[25]. Our resistance-gene-directed approach led to rediscovery of this compound with DHAD as a potential target. We first confirmed that aspterric acid is able to potently inhibit *A. thaliana* growth in an agar-based assay (Fig. 2a, Supplementary Fig. 5). Aspterric acid was also an effective inhibitor of root development and plant growth when applied to a representative monocot (*Zea mays*) and dicot (*Solanum lycopersicum*) (Fig. 2b). To test whether aspterric acid indeed targets DHAD, we expressed and purified housekeeping DHAD from both *A. terreus* (XP_001208445.1, *Ate*DHAD) and *A. thaliana* (AT3G23940, *Ath*DHAD), as well as the putative self-resistance enzyme AstD (Supplementary Fig. 6). Both housekeeping DHAD enzymes converted dihydroxyisovalerate to ketoisovalerate (*Ath*DHAD: $k_{cat} = 1.2\ s^{-1}$, $K_M = 5.7$ mM) as expected. The enzyme activities, however, were inhibited in the presence of aspterric acid (Extended Data Fig. 2). The half-maximal inhibitory concentration (IC_{50}) values of aspterric acid towards *Ate*DHAD and *Ath*DHAD were 0.31 μM and 0.50 μM, respectively, at an enzyme concentration of 0.50 μM (Extended Data Fig. 3). Aspterric acid was further determined to be a competitive inhibitor of *Ath*DHAD with a $K_i = 0.30$ μM (Extended Data Fig. 3). Aspterric acid displayed no significant cytotoxicity towards human cell lines up to 500 μM concentration, consistent with the lack of DHAD in mammalian cells (Supplementary Fig. 7).

AstD catalyses the identical β-dehydration reaction as DHAD, albeit with a significantly slower turnover rate ($k_{cat} = 0.03\ s^{-1}$, $K_M = 5.4$ mM). However, the enzyme was not inhibited by aspterric acid, even at the solubility limit of 8 mM (Extended Data Fig. 3). To determine if AstD can confer resistance to aspterric acid-sensitive strains, we developed a yeast-based assay. The genome copy of DHAD encoded by *ILV3* was first deleted from the *S. cerevisiae* strain DHY *ΔURA3*, which resulted in an auxotroph that requires exogenous addition of Ile, Leu and Val to grow. We introduced either the gene encoding *Ate*DHAD or *astD* episomally into the *ILV3* knockout strain and found that both genes enabled the cells to grow in the absence of the three BCAAs (Extended Data Fig. 4). However, yeast cells expressing *Ate*DHAD were approximately 100 times more sensitive to aspterric acid (IC_{50} of 2 μM) compared to yeast expressing AstD (IC_{50} of 200 μM) (Fig. 2c). Collectively, the biochemical and genetic assays validated that aspterric acid is, to our knowledge, the first natural-product inhibitor of fungal and plant DHAD, and that AstD serves as the self-resistance enzyme in the *ast* biosynthetic gene cluster.

The (*R*)-α-hydroxyacid and (*R*)-configured β-ether oxygen moieties in aspterric acid mimic the (2*R*, 3*R*)-dihydroxy groups present in natural substrates such as dihydroxyisovalerate. The β-ether oxygen in aspterric acid is in a position to coordinate to the 2Fe–2S cluster that is a required cofactor in both fungal and plant DHAD[16,17]. To understand the potential mechanism of action of aspterric acid, we determined the crystal structure (2.11 Å) of *Ath*DHAD in complex with the 2Fe–2S cluster (holo-*Ath*DHAD) (Fig. 2d, Extended Data Fig. 5, Extended Data Table 1). We identified a binding chamber at the homodimer interface, similar to that found in the holo bacterial L-arabinonate dehydratase[26] (Fig. 2d). The interior of the chamber is positively charged (2Fe–2S and Mg^{2+}) whereas the entrance is lined with hydrophobic residues. The modelled binding mode of α,β-dihydroxyisovalerate and aspterric acid predicted by computational docking are shown in Fig. 2e. The pocket is sufficiently spacious to accommodate the bulkier aspterric

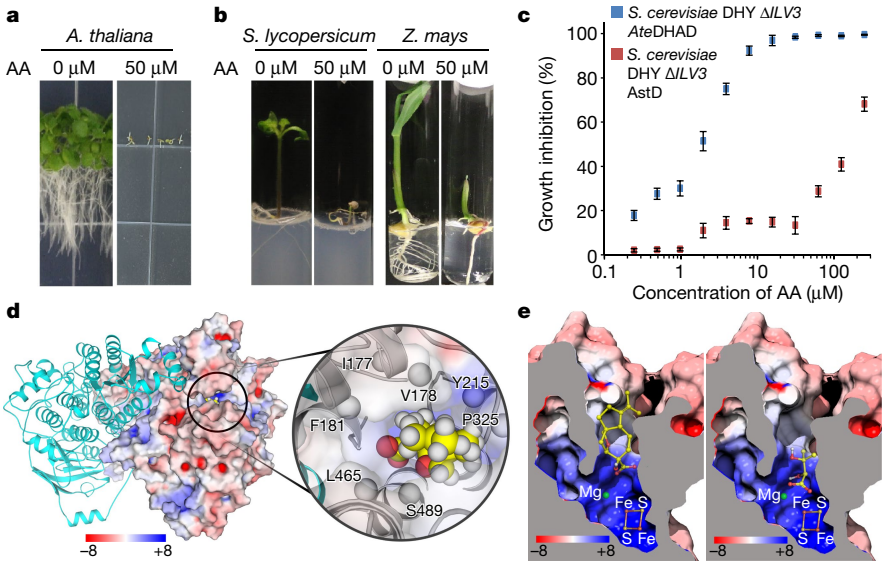

Fig. 2 | Aspteric acid is a plant growth inhibitor. a, Two-week-old *A. thaliana* growing on Murashige and Skoog basal medium containing no aspteric acid (left) or 50 μM aspteric acid (right). The picture shown is representative of three replicates. **b**, Same as in **a**, except for two-week-old dicotyledon *S. lycopersicum* and monocotyledon *Z. mays*. The picture shown is representative of two replicates. **c**, Verification of the self-resistance function of AstD. Growth-inhibition curve of aspteric acid on *S. cerevisiae* Δ*ILV3* strains expressing fungal housekeeping *Ate*DHAD (blue) or AstD (red) in isoleucine, leucine and valine (ILV) dropout medium. Data are mean ± s.d. from three biologically independent experiments. **d**, Crystal structure of dimeric holo-*Ath*DHAD containing the cofactor 2Fe–2S cluster and a Mg^{2+} ion with the docked aspteric acid in the active site. One of the *Ath*DHAD monomers is show in cyan, whereas the other one is shown in electrostatic surface representation. The docked aspteric acid is shown inset as a spaced-filled model. The hydrophobic portions of aspteric acid are surrounded by several hydrophobic residues (white spheres) from both monomers. **e**, Cross-section electrostatic map of modelled holo-*Ath*DHAD in the binding site. Red surface map, the normalized negatively charged regions; blue surface map, the normalized positively charged regions; white surface map, the hydrophobic regions. The docked aspteric acid in the active site of *Ath*DHAD is shown on the left, and the docked native substrate dihydroxyisovalerate is shown on the right. The docking studies suggest the hydrophobic entrance to the reaction chamber preferentially binds the bulkier, tricyclic aspteric acid.

acid, and provide stronger hydrophobic interactions than the native substrate with a 5.3 ± 0.3 kcal mol^{-1} gain in binding energy (Fig. 2e). On the basis of the holo-*Ath*DHAD structure, we constructed a homology model of AstD to determine the potential mechanism of resistance (Extended Data Figs. 5, 6). Comparison of *Ath*DHAD and the modelled AstD structures shows that although most of the residues in the catalytic chamber are conserved, the hydrophobic region at the entrance to the reactive chamber in AstD is more constricted as a result of two amino acid substitutions (V496L and I177L). Narrowing of the entrance could therefore sterically exclude the bulkier aspteric acid from binding in the active site, whereas the smaller, natural substrates are still able to enter the chamber.

To explore the potential of aspteric acid as an herbicide, we performed spray treatment of *A. thaliana* with aspteric acid. We added aspteric acid into a commercial glufosinate formulation known as Finale at a final concentration of 250 μM[27,28]. We then sprayed aspteric acid solution onto glufosinate-resistant *A. thaliana*. Finale alone had no observable inhibitory effects on plant growth, but adding aspteric acid severely inhibited plant growth (Extended Data Fig. 7). In addition, *A. thaliana* plants treated with aspteric acid before flowering failed to form normal pollen, which has also been observed previously[25]. We found that the pistil of treated plants could still be successfully pollinated using healthy pollen from the untreated *A. thaliana*, indicating that aspteric acid preferentially affects pollen but not egg formation (Extended Data Figs. 8, 9). This effect was also observed with a lower concentration of aspteric acid (100 μM). Thus, in addition to its herbicidal properties, aspteric acid could potentially be used as a chemical hybridization agent for hybrid seed production[29].

We next investigated whether plants expressing *astD* are resistant to aspteric acid. This was motivated by the successful combination of glyphosate and genetically modified crops that are selectively resistant to glyphosate (Roundup Ready)[30]. The *A. terreus astD* gene was codon optimized and the N terminus was fused to a chloroplast localization signal derived from *Ath*DHAD. Wild-type or *astD* transgene-expressing

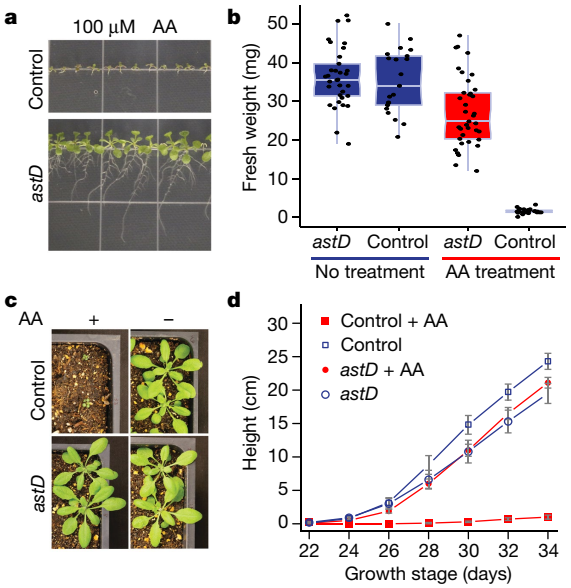

Fig. 3 | Aspteric acid-resistance of *Arabidopsis* plants expressing *astD* transgenes. a, Phenotype of ten-day-old *A. thaliana* with (lower) and without (upper) the *astD* transgene growing on medium containing 100 μM aspteric acid. Control plants were transformed with a vector that carries the glufosinate ammonium selection marker but no *astD* transgene. The picture shown is representative of three replicates. **b**, Fresh weight of three-week-old *Arabidopsis* seedlings growing on medium with (red box) and without (blue box) 100 μM aspteric acid. Box plots show the median and whiskers extend to the first and third quartiles, with the individual data points from 21 biologically independent experiments overlaid. **c**, Glufosinate-resistant *Arabidopsis* with (lower) and without (upper) *astD* transgene growing in soil were sprayed with glufosinate ammonium with (left) and without (right) 250 μM aspteric acid. **d**, Quantification of the height of *Arabidopsis* treated as in **c**. Data are mean ± s.d. from 12 biologically independent experiments.

A. thaliana was then grown on medium that contained 100 μM aspterric acid. In the presence of aspterric acid, the growth of wild-type plants was strongly inhibited, and arrested at the cotyledon stage (Fig. 3a). By contrast, the growth of *astD* transgenic plants was relatively unaffected by aspterric acid, as indicated by the normally expanded rosette leaves, elongated roots and whole-plant fresh weight (Fig. 3a, b). The expression of AstD was verified by western blot (Supplementary Fig. 8). A spray assay was also performed using T2 *astD* transgenic *A. thaliana* plants, which showed no observable growth defects under such treatment (Fig. 3c). By contrast, the control plants carrying the empty vector showed a strong growth inhibitory phenotype when treated with aspterric acid (Fig. 3c). Quantitative measurements of plant height showed that AstD effectively confers aspterric acid resistance to *A. thaliana* (Fig. 3d).

In summary, resistance-gene-directed discovery of natural products in the fungus *A. terreus* led to the discovery of a natural herbicide aspterric acid and the determination of its mode of action. In addition, introducing *astD* as a transgene or editing the sequence of the plant DHAD endogenous gene could be used to create aspterric acid-resistant crops. We suggest that aspterric acid is a promising lead for development as a broad spectrum commercial herbicide.

Online content

Any Methods, including any statements of data availability and Nature Research reporting summaries, along with any additional references and Source Data files, are available in the online version of the paper at https://doi.org/10.1038/s41586-018-0319-4

Received: 21 November 2017; Accepted: 22 May 2018;
Published online 11 July 2018.

1. Dayan, F. E. & Duke, S. O. Natural compounds as next-generation herbicides. *Plant Physiol*. **166**, 1090–1105 (2014).
2. Newman, D. J. & Cragg, G. M. Natural products as sources of new drugs from 1981 to 2014. *J. Nat. Prod*. **79**, 629–661 (2016).
3. Clardy, J. & Walsh, C. Lessons from natural molecules. *Nature* **432**, 829–837 (2004).
4. Ziemert, N., Alanjary, M. & Weber, T. The evolution of genome mining in microbes—a review. *Nat. Prod. Rep*. **33**, 988–1005 (2016).
5. Clevenger, K. D. et al. A scalable platform to identify fungal secondary metabolites and their gene clusters. *Nat. Chem. Biol*. **13**, 895–901 (2017).
6. Rutledge, P. J. & Challis, G. L. Discovery of microbial natural products by activation of silent biosynthetic gene clusters. *Nat. Rev. Microbiol*. **13**, 509–523 (2015).
7. Tang, X. et al. Identification of thiotetronic acid antibiotic biosynthetic pathways by target-directed genome mining. *ACS Chem. Biol*. **10**, 2841–2849 (2015).
8. Alanjary, M. et al. The antibiotic resistant target seeker (ARTS), an exploration engine for antibiotic cluster prioritization and novel drug target discovery. *Nucleic Acids Res*. **45**, W42–W48 (2017).
9. Yeh, H.-H. et al. Resistance gene-guided genome mining: serial promoter exchanges in *Aspergillus nidulans* reveal the biosynthetic pathway for fellutamide B, a proteasome inhibitor. *ACS Chem. Biol*. **11**, 2275–2284 (2016).
10. Amorim Franco, T. M. & Blanchard, J. S. Bacterial branched-chain amino acid biosynthesis: structures, mechanisms, and drugability. *Biochemistry* **56**, 5849–5865 (2017).
11. Heap, I. Global perspective of herbicide-resistant weeds. *Pest Manag. Sci*. **70**, 1306–1315 (2014).
12. Soltani, N. et al. Potential corn yield losses from weeds in North America. *Weed Technol*. **30**, 979–984 (2016).
13. Swanton, C. J., Harker, K. N. & Anderson, R. L. Crop losses due to weeds in Canada. *Weed Technol*. **7**, 537–542 (1993).
14. Gianessi, L. P. The increasing importance of herbicides in worldwide crop production. *Pest Manag. Sci*. **69**, 1099–1105 (2013).
15. Flint, D. H. & Emptage, M. H. Dihydroxy acid dehydratase from spinach contains a [2Fe–2S] cluster. *J. Biol. Chem*. **263**, 3558–3564 (1988).
16. Flint, D. H., Emptage, M. H., Finnegan, M. G., Fu, W. & Johnson, M. K. The role and properties of the iron–sulfur cluster in *Escherichia coli* dihydroxy-acid dehydratase. *J. Biol. Chem*. **268**, 14732–14742 (1993).
17. Flint, D. H. & Nudelman, A. Studies on the active site of dihydroxy-acid dehydratase. *Bioorg. Chem*. **21**, 367–385 (1993).
18. Pusztahelyi, T., Holb, I. J. & Pócsi, I. Secondary metabolites in fungus–plant interactions. *Front. Plant Sci*. **6**, 573 (2015).
19. Kennedy, J. et al. Modulation of polyketide synthase activity by accessory proteins during lovastatin biosynthesis. *Science* **284**, 1368–1372 (1999).
20. Regueira, T. B. et al. Molecular basis for mycophenolic acid biosynthesis in *Penicillium brevicompactum*. *Appl. Environ. Microbiol*. **77**, 3035–3043 (2011).
21. Fischbach, M. A. & Walsh, C. T. Assembly-line enzymology for polyketide and nonribosomal peptide antibiotics: logic, machinery, and mechanisms. *Chem. Rev*. **106**, 3468–3496 (2006).
22. Christianson, D. W. Structural biology and chemistry of the terpenoid cyclases. *Chem. Rev*. **106**, 3412–3442 (2006).
23. Tang, M.-C. et al. Discovery of unclustered fungal indole diterpene biosynthetic pathways through combinatorial pathway reassembly in engineered yeast. *J. Am. Chem. Soc*. **137**, 13724–13727 (2015).
24. Yoshisuke Tsuda et al. Aspterric acid, a new sesquiterpenoid of the carotane group, a metabolite from *Aspergillus terreus* IFO-6123. X-ray crystal and molecular structure of its p-bromobenzoate. *J. Chem. Soc. Chem. Commun*. **0**, 160–161 (1978).
25. Shimada, A. et al. Aspterric acid and 6-hydroxymellein, inhibitors of pollen development in *Arabidopsis thaliana*, produced by *Aspergillus terreus*. *Z. Naturforsch. C* **57**, 459–464 (2002).
26. Rahman, M. M. et al. The crystal structure of a bacterial l-arabinonate dehydratase contains a [2Fe–2S] cluster. *ACS Chem. Biol*. **12**, 1919–1927 (2017).
27. Kirkwood, R. C. Use and mode of action of adjuvants for herbicides: a review of some current work. *Pestic. Sci*. **38**, 93–102 (1993).
28. Hoerlein, G. Glufosinate (phosphinothricin), a natural amino acid with unexpected herbicidal properties. *Rev. Environ. Contam. Toxicol*. **138**, 73–145 (1994).
29. McRae, D. H. in *Plant Breeding Reviews* (ed. Janick, J.) 169–191 (John Wiley & Sons, New Jersey, 1985).
30. Benbrook, C. M. Trends in glyphosate herbicide use in the United States and globally. *Environ. Sci. Eur*. **28**, 3–19 (2016).

Acknowledgements This work was supported by the NIH (1DP1GM106413 and 1R35GM118056) to Y.T. and CAS (XDB20000000) to J.Z. S.E.J. is an Investigator of the Howard Hughes Medical Institute. Q.L. is supported by the NIH (F32) Postdoctoral Fellowship. We thank Stanford Genome Technology Center for the *S. cerevisiae* DHY *ΔURA3* strain. The diffraction data of holo-*Ath*DHAD was collected at beamline BL19U1 of the Shanghai Synchrotron Radiation Facility (SSRF). The molecular modelling was performed at the Interdisciplinary Centre for Mathematical and Computational Modeling in Warsaw (GB70-3 & GB71-3). We thank W. Huang, L. Wu and R. Cheng for technical help with protein purification and crystallization.

Reviewer information *Nature* thanks F. Dayan, E. Sattely and the other anonymous reviewer(s) for their contribution to the peer review of this work.

Author contributions Y.Y., Q.L., J.Z., S.E.J. and Y.T. developed the hypothesis and designed the study. Y.Y. performed all in vivo and in vitro experiments. Q.L., Y.Y. and C.N. performed plant experiments. X.Z. and J.Z. performed crystallography experiments. J.G. determined the protein structure. S.Y. performed computational experiments. Y.Y. and U.B.-E. performed yeast experiments. Y.Y., Q.L., J.Z., S.E.J. and Y.T. prepared the manuscript.

Competing interests A PCT patent application related to this manuscript has been filed by UCLA.

Additional information
Extended data is available for this paper at https://doi.org/10.1038/s41586-018-0319-4.
Supplementary information is available for this paper at https://doi.org/10.1038/s41586-018-0319-4.
Reprints and permissions information is available at http://www.nature.com/reprints.
Correspondence and requests for materials should be addressed to J.Z., S.E.J. and Y.T.
Publisher's note: Springer Nature remains neutral with regard to jurisdictional claims in published maps and institutional affiliations.

METHODS

No statistical methods were used to predetermine sample size. The experiments were not randomized and the investigators were not blinded to allocation during experiments and outcome assessment.

Materials. Biological reagents, chemicals, media and enzymes were purchased from standard commercial sources unless stated. The plant, fungal, yeast and bacterial strains, plasmids and primers used in this study are summarized in Supplementary Tables 3, 4 and 5. DNA and RNA manipulations were carried out using Zymo ZR Fungal/Bacterial DNA Microprep kit and Invitrogen Ribopure kit respectively. DNA sequencing was performed at Laragen. The primers and codon-optimized gblocks were synthesized by IDT.

Expression of *ast* genes in *Aspergillus nidulans* for cDNA isolation. Plasmids pYTU, pYTP, pYTR were digested with *Pac*I and *Swa*I and used as vectors to insert genes[31]. A *gpda* promoter was generated by PCR amplification using primers Gpda-pYTU-F and Gpda-R with pYTR serving as template. Genes to be expressed were amplified using PCR with the genomic DNA of *A. terreus* NIH2624 as a template. A 4.5-kb fragment obtained using primers AstD-pYTU-recomb-F and AstA-pYTU-recomb-R was cloned into pYTU together with a *gpda* promoter by yeast homologous recombination to obtain pAstD+AstA-pYTU. Yeast transformation was performed using Frozen-EZ Yeast Transformation II Kit (Zymo Research). A 2.4-kb fragment obtained using primers AstB-pYTR-recomb-F and AstB-pYTR-recomb-R was cloned into pYTR by yeast homologous recombination to obtain pAstB-pYTR. Similarly, a 2.3-kb fragment obtained using primers AstC-pYTP-recomb-F and AstC-pYTP-recomb-R was cloned into pYTP by yeast homologous recombination to obtain pAstC-pYTP.

All three plasmids (pAstD+AstA-pYTU, pAstB-pYTR and pAstC-pYTP) were transformed into *A. nidulans* according to standard protocols to result in the *A. nidulans* strain TY01[31]. TY01 was cultured in liquid CD-ST medium (20 g l^{-1} starch, 20 g l^{-1} peptone, 50 ml l^{-1} nitrate salts and 1 ml l^{-1} trace elements) at 28 °C for 3 days. Total RNA of TY01 was extracted with the Invitrogen Ribopure kit, and total cDNA of TY01 was obtained using the SuperScript III reverse transcriptase kit (Thermo Fisher Scientific). The cDNA fragment of *astA* was PCR amplified using primers AstA-xw55-recomb-F and AstA-xw55-recomb-R. The cDNA fragment of *astB* was PCR amplified using primers AstB-xw06-recomb-F and AstB-xw06-recomb-R. The cDNA fragment of *astC* was PCR amplified using primers AstC-xw02-recomb-F and AstC-xw02-recomb-R. The cDNA fragment of *astD* was PCR amplified using primers AstD-pXP318-F and AstD-pXP318-R. All the introns were confirmed to be correctly removed by sequencing.

Construction of *S. cerevisiae* strains. Plasmid pXW55 (*URA3* marker) digested with *Nde*I and *Pme*I was used to introduce the *astA* gene[23] into *S. cerevisiae* RC01. A 1.3-kb fragment containing *astA* obtained from PCR using primers AstA-xw55-recomb-F and AstA-xw55-recomb-R was cloned into pXW55 using yeast homologous recombination to produce pAstA-xw55. The plasmid pAstA-xw55 was then transformed into *S. cerevisiae* RC01 to generate strain TY02[23].

Plasmid pXW06 (*TRP1* marker) digested with *Nde*I and *Pme*I was used to introduce the *astB* gene[23] *S. cerevisiae* RC01. A 1.6-kb fragment containing *astB* obtained from PCR using primers AstB-xw06-recomb-F and AstB-xw06-recomb-R were cloned into pXW06 using yeast homologous recombination to produce pAstB-xw06. The plasmid pAstB-xw06 was then transformed into TY02 to generate strain TY03.

Plasmid pXW06 (*LEU2* marker) digested with *Nde*I and *Pme*I was used to introduce the *astC* gene[23] *S. cerevisiae* RC01. A 1.6-kb fragment containing *astC* obtained from PCR using primers AstC-xw02-recomb-F and AstC-xw02-recomb-R were cloned into pXW02 using yeast homologous recombination to produce pAstC-xw02. The plasmid pAstC-xw02 was then transformed into TY03 to generate strain TY04.

The *URA3* gene was inserted into the *ILV3* locus of *S. cerevisiae* DHY Δ*URA3* strain to generate UB01. A 879-bp homologous-recombination donor fragment with 35–40 bp homologous regions flanking the *ILV3* ORF was amplified using primers ILV3p-URA3-F and ILV3t-URA3-R using yeast gDNA as a template. The PCR product was gel purified and transformed into *S. cerevisiae* DHY Δ*URA3*, and selected on uracil dropout medium to give UB01. The resulting strain was subjected to verification using colony PCR with primers ILV3KO-ck-F and ILV3KO-ck-R and the amplified fragment was confirmed with sequencing.

The *URA3* gene inserted into the *ILV3* locus of *S. cerevisiae* DHY Δ*URA3* was deleted from UB01 using homologous recombination to generate UB02. A 150-bp homologous-recombination donor fragment with 75-bp homologous regions flanking the *ILV3* ORF was amplified using primers ILV3KO-F and ILV3KO-R, gel purified, transformed into UB01, and counter-selected on 5-fluoroorotic acid (5-FoA)-containing medium to give UB02. The resulting strain was subjected to verification using colony PCR with primers ILV3KO-ck-F and ILV3KO-ck-R and the amplified fragment was confirmed with sequencing.

The empty plasmid pXP318 (*URA3* marker) was transformed into UB02 to generate TY05[32].

Plasmid pXP318 digested with *Spe*I and *Xho*I was used as vector to introduce the gene encoding *Ate*DHAD[32] into the plasmid UB02. The cDNA of *A. terreus* NIH 2624 served as the template for PCR amplification. A 1.7-kb fragment obtained using primers *Ate*DHAD-pXP318-F and *Ate*DHAD-pXP318-R were cloned into pXP318 using yeast homologous recombination to produce *Ate*DHAD-pXP318. Then, *Ate*DHAD-pXP318 was transformed into UB02 to generate TY06. *Ate*DHAD was driven by a constitutive *TEF1* promoter.

Plasmid pXP318 digested with *Spe*I and *Xho*I was used as vector to introduce the *astD* gene[32] into the plasmid UB02. The cDNA isolated from TY01 served as the template for PCR amplification. A 1.8-kb fragment obtained using primers AstD-pXP318-F and AstD-pXP318-R were cloned into pXP318 using yeast homologous recombination to make AstD-pXP318. A Flag tag was also added to the N-terminal of AstD. AstD-pXP318 was then transformed into UB02 to generate TY07. AstD was driven by the constitutive *TEF1* promoter.

Fermentation and compound analyses and isolation. A seed culture of *S. cerevisiae* strain was grown in 40 ml of synthetic dropout medium for 2 days at 28 °C, 250 r.p.m. Fermentation of the yeast was carried out using YPD (yeast extract 10 g l^{-1}, peptone 20 g l^{-1}) supplemented with 2% dextrose for 3 days at 28 °C, 250 r.p.m.

HPLC–MS analyses were performed using a Shimadzu 2020 EVLC-MS (Phenomenex Luna, 5μ, 2.0 × 100 mm, C-18 column) with positive and negative mode electrospray ionization. The elution method was a linear gradient of 5–95% (v/v) acetonitrile/water over 15 min, and then 95% (v/v) acetonitrile/water for 3 min with a flow rate of 0.3 ml min^{-1}. The HPLC buffers were supplemented with 0.05% formic acid (v/v). HPLC purifications were performed using a Shimadzu Prominence HPLC (Phenomenex Kinetex, 5μ, 10.0 × 250 mm, C-18 column). The elution method was a linear gradient of 65–100% (v/v) acetonitrile/water in 25 min, with a flow rate of 2.5 ml min^{-1}. Gas chromatography–mass spectrometry (GC–MS) analyses were performed using Agilent Technologies GC–MS 6890/5973 equipped with a DB-FFAP column. An inlet temperature of 240 °C and constant pressure of 4.2 psi were used. The oven temperature was initially set at 60 °C, then ramped up at 10 °C min^{-1} for 20 min and finally held at 240 °C for 5 min.

To isolate compound **1**, the fermentation broth of TY02 was centrifuged (5,180*g*, 10 min), and the cell pellet was collected and soaked in acetone. The organic phase was dried over sodium sulfate, concentrated to oil form and subjected to silica column purification with hexane. To isolate compound **2**, the fermentation broth of TY03 was centrifuged (5,180*g*, 10 min), and the supernatant was extracted three times with ethyl acetate. The organic phase was dried over sodium sulfate, concentrated to oil form, and then and subjected to HPLC purification. To isolate aspterric acid, the fermentation broth of TY04 was centrifuged (5,180*g*, 10 min), and supernatant was extracted three times with ethyl acetate. The organic phase was dried over sodium sulfate, concentrated to oil form, and subjected to HPLC purification.

Structure determination of compounds. Compound **1**, a colourless oil that readily dissolved in hexane and chloroform, had a molecular formula $C_{15}H_{24}$, as deduced from electron ionization–mass spectrometry (EI–MS) $[M]^+$ *m/z* 204, and showed $[\alpha]_D^{22} = -30°$ (*n*-hexane; $c = 0.1$). GC–MS 70 eV, *m/z* (relative intensity): 204 $[M]^+$ (42), 189 (5), 161 (35), 136 (100), 133 (10), 121 (70), 119 (25), 107 (20), 105 (27), 93 (21), 91 (26), 79 (13), 77 (15), 69 (20), 55 (12), 43 (12), 41 (13), 38 (21); ^{1}H NMR (500 MHz, $CDCl_3$): δ (p.p.m.) 5.37 (1H, m), 2.20–2.10 (5H, m), 2.10–2.00 (2H, m), 1.95 (1H, d, 15.3), 1.75 (3H, s), 1.71 (3H, q, 1.7), 1.61 (3H, br s), 1.44 (1H, dd, 11.4, 7.2), 1.36 (1H, m), 1.31 (1H, dd, 11.3, 2.6), 0.73 (3H, s); ^{13}C NMR (125 MHz, $CDCl_3$): δ 138.4, 138.3, 122.4, 122.2, 57.4, 42.6, 41.4, 40.3, 34.5, 29.6, 27.3, 25.0, 23.3, 20.6, 19.2. Both of the NMR and mass spectrometry spectra are identical to a known compound (+)-daucane, however, the optical rotation is opposite which led to the assignment of **1** to be (−)-daucane[33].

Compound **2**, a colourless oil that readily dissolved in ethyl acetate and chloroform, had a molecular formula $C_{15}H_{22}O_3$, as deduced from liquid chromatography–mass spectrometry (LC–MS) $[M+H]^+$ *m/z* 251, $[M-H]^-$ *m/z* 249. ^{1}H NMR (500 MHz, $CDCl_3$): δ 8.09 (1H, brs), 3.25 (1H, t, 7.4), 2.71 (1H, dd, 14.6, 6.5), 2.48 (1H, dd, 14.8, 6.3), 2.36 (1H, dd, 14.0, 6.6), 2.26 (1H, m), 2.15 (1H, dd, 16.3, 8.9), 2.08 (1H, d, 12.0), 1.84 (1H, q, 13.1), 1.73 (3H, d, 2.3), 1.59 (3H, d, 2.2), 1.48–1.35 (3H, m), 1.31 (1H, td, 11.5, 9.0), 0.86 (3H, s). ^{13}C NMR (125 MHz, $CDCl_3$): δ 176.0, 135.8, 123.2, 60.1, 59.8, 59.4, 44.1, 40.5, 38.8, 30.6, 29.3, 24.9, 23.8, 20.6, 17.8.

Compound **3**, a colourless oil that readily dissolved in acetone and chloroform, had a molecular formula $C_{15}H_{22}O_4$, as deduced from LC–MS $[M+H]^+$ *m/z* 267, $[M-H]^-$ *m/z* 265. ^{1}H NMR (500 MHz, $CDCl_3$): δ 4.29 (1H, d, 8.5), 3.92 (1H, d, 8.3), 3.48 (1H, d, 8.3), 2.42 (1H, dd, 14.9, 7.3), 2.37–2.28 (2H, m), 2.25 (1H, dd, 13.0, 4.4), 2.20–2.17 (1H, m), 2.12 (1H, d, 13.4), 2.01 (1H, m), 1.80–1.65 (2H, m), 1.71 (3H, s), 1.64–1.54 (1H,m), 1.60 (3H, s), 1.50 (1H, m); ^{13}C NMR (125 MHz, $CDCl_3$): δ 178.2, 134.5, 125.2, 82.9, 76.3, 75.6, 55.4, 53.0, 36.6, 36.2, 33.8, 32.2, 23.6, 23.4, 20.9. Compound **3** is identical to aspterric acid as reported[24,25].

Protein expression, purification and biochemical assay. To express and purify *Ath*DHAD, primers *Ath*DHAD-pET-F and *Ath*DHAD-pET-R were used to amplify a 1.7-kb DNA fragment containing *Ath*DHAD (AT3G23940). The PCR

product was cloned into pET28a using *Nhe*I and *Not*I restriction sites. The resulting plasmid *Ath*DHAD-pET was transformed into *E.coli* BL21 (DE3) to give TY08. To express and purify *Ate*DHAD (XP_001208445.1), primers *Ate*DHAD-pET-F and *Ate*DHAD-pET-R were used to amplify a 1.6-kb DNA fragment containing *Ate*DHAD. The PCR product was cloned into pET28a using *Nde*I and *Not*I restriction sites. The resulting plasmid *Ate*DHAD-pET was transformed into *E. coli* BL21 (DE3) to obtain TY09. To express and purify AstD (XP_001213593.1), primers AstD-pET-F and AstD-pET-R were used to amplify a 1.6-kb DNA fragment containing *astD*. The PCR product was cloned into pET28a using *Nde*I and *Not*I restriction sites. The resulting plasmid AstD-pET was transformed into *E. coli* BL21 (DE3) to obtain TY10. All DHADs with a fused 6 × His-tag with a molecular mass of ~62 kDa were expressed at 16 °C 220 rpm for 20 h after 100 μM isopropyl β-D-1-thiogalactopyranoside IPTG induction (IPTG was added when $OD_{600\,nm} = 0.8$). Cells from a 1-l culture were then collected by centrifugation at 5,180*g* at 4 °C. Cell pellet was resuspended in 15 ml Buffer A10 (20 mM Tris-HCl pH 7.5, 50 mM NaCl, 8% glycerol, 10 mM imidazole). The cells were lysed by sonication, and the insoluble material was sedimented by centrifugation at 35,267*g* at 4 °C. The protein supernatant was then incubated with 3 ml Ni–NTA for 4 h with slow, constant rotation at 4 °C. Subsequently the Ni–NTA resin was washed with ten column volumes of Buffer A50 (Buffer A with 50 mM imidazole). For elution of the target protein, the Ni–NTA resin was incubated for 10 min with 6 ml Buffer A300 (Buffer A with 300 mM imidazole). The supernatant from the elution step was then analysed by SDS–PAGE together with the supernatants from the other purification steps. The elution fraction containing the recombinant protein was buffer exchanged into storage buffer (50 mM Tris-HCl pH 7.2, 50 mM NaCl, 10 mM $MgCl_2$, 10% glycerol, 5 mM DTT, 5 mM GSH).

In vitro activity assays were carried out in 50 μl reaction mixture containing storage buffer, 10 mM (±)-sodium α,β-dihydroxyisovalerate hydrate (**4**) and 0.5 μM of purified DHAD enzyme. The reaction was initiated by adding the enzyme. After 0.5 h incubation at 30 °C, the reactions were stopped by adding an equal volume of ethanol. Approximately 0.1 volumes of 100 mM phenylhydrazine (PHH) was added to derivatize the product 3-methyl-2-oxo-butanoic acid (**5**) into **6** at room temperature for 30 min. 20 μl of the reaction mixture was used for the LC–MS analysis. The area of the HPLC peak with UV absorption at 350 nm were used to quantify the amount of **6**. (Extended Data Fig. 2).

The inhibition percentage of aspteric acid on DHADs was determined using in vitro biochemical assays and calculated with following equation:

$$\text{inhibition percentage} = 1 - \frac{\text{initial reaction rate with aspteric acid}}{\text{initial reaction rate without aspteric acid}}$$

Growth inhibition assay of *S. cerevisiae* on plates or in the tubes. *S. cerevisiae* was grown in isoleucine, leucine and valine (ILV) dropout medium (20 g l^{-1} glucose, 0.67 g l^{-1} Difco Yeast Nitrogen Base without amino acids, 18 mg l^{-1} adenine, arginine 76 mg l^{-1}, asparagine 76 mg l^{-1}, aspartic acid 76 mg l^{-1}, glutamic acid 76 mg l^{-1}, histidine 76 mg l^{-1}, lysine 76 mg l^{-1}, methionine 76 mg l^{-1}, phenylalanine 76 mg l^{-1}, serine 76 mg l^{-1}, threonine 76 mg l^{-1}, tryptophan 76 mg l^{-1}, tyrosine 76 mg l^{-1}) to test growth inhibition of aspteric acid on *S. cerevisiae*, cells were incubated at 28 °C until $OD_{600\,nm}$ of the control strain without aspteric acid treatment reached about 0.8. The ratio of yeast $OD_{600\,nm}$ in medium with aspteric acid treatment to yeast OD_{600} in medium without aspteric acid was calculated as the percentage of growth inhibition. The inhibition curve was plotted as the percentage of inhibition versus aspteric acid concentrations. To further prove aspteric acid affects BCAA biosynthesis, isoleucine, leucine and valine were also complemented to the medium with or without treatment with aspteric acid. The growth curves of TY05, TY06 and TY07 were also plotted in Extended Data Fig. 4. The $OD_{600\,nm}$ was recorded for every 20 min over a total of 50 h. The growth inhibition percentage of aspteric acid on *S. cerevisiae* strain is calculated by dividing the cell density ($OD_{600\,nm}$) of the aspteric acid-treated strain to the corresponding untreated strains when $OD_{600\,nm}$ reaches approximately 0.8 using the following equation:

$$\text{growth inhibition percentage} = 1 - \frac{\text{OD}_{600\,nm}\text{ of }\mathbf{AA}\text{ treated strain}}{0.8}$$

in which 0.8 is the $OD_{600\,nm}$ of the untreated strain.

Growth inhibition assay of plants on plates or in the tubes. MS (2.16 g l^{-1} Murashige and Skoog basal medium, 8 g l^{-1} sucrose, 8 g l^{-1} agar) medium was used to test the growth inhibition of aspteric acid on *A. thaliana*, *S. lycopersicum* and *Z. mays*. *A. thaliana*, *S. lycopersicum* and *Z. mays* were grown under long day condition (16/8 h light/dark) using cool-white fluorescence bulbs as the light resource at 23 °C. Aspteric acid was dissolved in ethanol and added to the medium before inoculating strains or growing plants. The medium of the control treatment contained the same amount of ethanol, but without aspteric acid.

Plant growth inhibition assay by spraying. Aspteric acid was first dissolved in ethanol and then added to solvent (0.06 g l^{-1} Finale (Bayer) with 20 g l^{-1} EtOH). The control plants were treated with solvent containing ethanol only. *A. thaliana* that are resistant to glufosinate (containing the *bar* gene) were grown under long day condition (16/8 h light/dark) using cool-white fluorescence bulbs as the light resource at 23 °C. Spraying treatments began upon seed germination and were repeated once every two days with approximately 0.4 ml aspteric acid solution each time per pot.

Structure determination of holo-*Ath*DHAD. The gene encoding *Ath*DHAD (residues 35–608) was cloned into pET21a derivative vector pSJ2 with an eight histidine (8 × His) tag and a TEV protease cleavage site at the N-terminus. The forward primer DHAD-F and the reverse primer DHAD-R were used for cloning. The double mutant K559A/K560A for efficient crystallization was designed using the surface entropy reduction prediction (SERp) server[34]. Mutations were generated by PCR using the forward primer K559AK560A-F and reverse primer K559AK560A-R. All constructed plasmids were verified by DNA sequencing.

*Ath*DHAD purified under aerobic conditions was found to contain no iron–sulfur cluster (apo form). Hence we performed [2Fe–2S] cluster reconstitution under the atmosphere of nitrogen in an anaerobic box. The protein was incubated with $FeCl_3$ at the ratio of 1:10 for 1 h on ice and then 10 equivalents of Na_2S per protein was added drop-wise every 30 min for 3 h. The reaction mixture was then incubated overnight. Excess $FeCl_3$ and Na_2S were removed using a SephadexTM G-25 Fine column (GE Healthcare)[26].

The reconstituted holo-*Ath*DHAD was crystallized in an anaerobic box. The proteins (at 10 mg ml^{-1}) were mixed in a 1:1 ratio with the reservoir solution in a 2-μl volume and equilibrated against 50 μl reservoir solution, using the sitting-drop vapour diffusion method at 16 °C. Crystals for diffraction were observed in 0.1 M sodium acetate pH 5.0, 1.5 M ammonium sulfate after 5 days.

All crystals were flash-cooled in liquid nitrogen after cryo-protection with a solution containing 25% glycerol, 1.5 M ammonium sulfate, 0.1 M sodium acetate pH 5.0. The data were collected at 100 K at the Beam Line 19U1 in the Shanghai Synchrotron Radiation Facility (SSRF). Diffraction data of holo-*Ath*DHAD were collected at the wavelength of 0.97774 Å. The best crystals diffracted to a resolution of 2.11 Å. The Ramachandran plot favoured (%), allowed (%) and outlier (%) are 98.05, 1.60, and 0.36, respectively. All datasets were indexed, integrated, and scaled using the HKL3000 package[35]. The crystals belonged to space group $P4_22_12$. The statistics of the data collection are summarized in Extended Data Table 1.

The holo-*Ath*DHAD structure was solved using the molecular replacement method Phaser embedded in the CCP4i suite and the L-arabinonate dehydratase crystal structure (RCSB Protein Data Bank (PDB) ID: 5J83) as the search model. All the side chains were removed during the molecular replacement process[36,37]. The resulting model was refined against the diffraction data using the REFMAC5 program of CCP4i[38]. On the basis of the improved electron density, the side chains of the holo-*Ath*DHAD protein, iron–sulfur cluster, water molecule, acetate ion, sulfate ions, and magnesium ion were manually built using the program WinCoot[39]. The R_{work} and R_{free} values of the structure are 17.27% and 21.52%, respectively. The detailed refinement statistics are summarized in Extended Data Table 1. The geometry of the model was validated by WinCoot. Structural factor and coordinate of holo-*Ath*DHAD have been deposited in the Protein Data Bank (PDB ID: 5ZE4).

Homology modelling of AstD and docking of substrate or aspteric acid into the active site of holo-*Ath*DHAD. The structure of holo-*Ath*DHAD was prepared using Schrodinger suite software under an OPLS3 force field[40]. Hydrogen atoms were added to reconstituted crystal structures according to the physiological pH (7.0) with the PROPKA tool in Protein Preparation tool in Maestro to optimize the hydrogen bond network[26,41]. Constrained energy minimizations were conducted on the full-atomic models, with heavy atom coverage to 0.5 Å. The homology model was performed in Modeller 9.18[42], using the crystal structure of holo-*Ath*DHAD solved in this work as a template. Sequence alignment in Modeller indicated that AstD and *Ath*DHAD shared 56.8% sequence identity and 75.0% sequence similarity (Extended Data Fig. 6). All the highly conserved residues and motifs were properly aligned. A total of 2,000 models were generated for each target in Modeller with the fully annealed protocol. The optimal models were chosen for docking studies according to DOPE (Discrete Optimized Protein Energy) score.

All ligand structures were built in Schrodinger Maestro software[26]. The LigPrep module in Schrodinger software was introduced for geometric optimization by using an OPLS3 force field[40]. The ionization states of ligands were calculated with Epik tool using Hammett and Taft methods in conjunction with ionization and tautomerization tools[43]. The docking of a ligand to the receptor was performed using Glide[44]. We included cofactors observed in the crystal structure during the docking. As both water and SO_4^{2-} occupied the catalytic site, they were excluded before docking. Cubic boxes centred on the ligand mass centre with a radius of 8 Å for all ligands defined the docking binding regions. Flexible ligand docking was executed for all structures. Ten poses per ligand out of 20,000 were included in the post-docking energy minimization. The best scored pose for the ligand was chosen as the initial structure for further study. The molecular mechanics energies combined with the generalized Born and surface area continuum solvation

(MM/GBSA) method was introduced to evaluate the ligand binding affinity on the basis of the best-scored docking pose in Schrodinger software. Figures were prepared in PyMOL and Inkscape[45,46]. Both the native substrate α,β-dihydroxyisovalerate and aspterric acid were docked into the catalytic site of *Ath*DHAD. The cross-section electrostatic surface map shows this unique catalytic pocket has a positively charged interior and a hydrophobic entrance, which binds to negatively charged 'head' and hydrophobic 'tail' of the substrate or aspterric acid, respectively. Thus the negatively charged 'head' can lead both of the substrate and aspterric acid into the catalytic chamber. The bulky hydrophobic tricyclic moiety of aspterric acid, however, provides stronger hydrophobic interactions to the entrance and blocks the entrance of the active site owing to the hydrophobic residues at the entrance (Fig. 2d). By contrast, the smaller 'tail' of the native substrate provides fewer interactions to the entrance because the smaller size limits efficient hydrophobic contact to nearby residues. This implies that once aspterric acid binds to *Ath*DHAD, it can prevent the substrate approaching the active site. We also introduced the MM/GBSA method, a widely used approach for relative binding energy calculation, to evaluate the relative binding affinity for both ligands[47]. The MM/GBSA calculations were done in Prime[48] (Schrödinger 2015 suite). The MM/GBSA energy was calculated using following equation, $\Delta G_{bind} = E_{complex} - E_{protein} - E_{ligand}$. E denotes energy and includes terms such as protein−ligand van der Waals contacts, electrostatic interactions, ligand desolvation, and internal strain (ligand and protein) energies, using a VSGB2.0 implicit solvent model with the OPLS2005 force field. The solvent entropy is also included in the VSGB2.0 energy model, as it is for other generalized Born and Poison−Boltzmann continuum solvent models.

MM/GBSA calculation shows that the relative binding energy for aspterric acid and α,β-dihydroxyisovalerate is -18.6 ± 0.3 kcal mol^{-1} and -13.3 ± 0.2 kcal mol^{-1}, respectively, which shows that the binding constant of aspterric acid to the active site is about 6,000 times greater than α,β-dihydroxyisovalerate. This further confirms that aspterric acid is a competitive inhibitor of *Ath*DHAD.

Cytotoxicity assay of aspterric acid. Cell proliferation experiments were performed in a 96-well format (five replicates per sample) using the human melanoma cell lines A375 and SK-MEL-1. Aspterric acid treatments were initiated 24 h after seeding for 72 h, and cell survival was quantified using the CellTiter-GLO assay (Promega).

Cross experiment of *A. thaliana*. To make male sterile *A. thaliana*, aspterric acid was added to a chemical hybridization agent (CHA) formulation (250 μM aspterric acid, 2% ethanol, 0.1% Tween-80, 1% corn oil in water), which has less inhibition effect on the growth of *A. thaliana*. Flowers of the aspterric acid-treated Col-0 were selected as the female parent. The non-treated *A. thaliana* containing a glufosinate resistance gene were used as the male parent to donate pollen. Two-week-old F1 progeny resulting from the cross were treated by Finale (11.3% glufosinate-ammonium) at a 1:2,000 dilution. The results are summarized in Extended Data Fig. 9.

Construction of the transgenic plants. The coding sequence of AstD was codon optimized for *A. thaliana*. A chloroplast-localization signal (CLS) of 35 amino acid residues derived from the N-terminal of *A. thaliana* DHAD (MQATIFSPRATLFPCKPLLPSHNVNSRRPSIISCS) was fused to the N terminus of the codon-optimized AstD. A 3 × Flag-tag was inserted between the CLS and the codon-optimized AstD (Supplementary Table 6). The gene block containing CLS, the Flag-tag and *astD* was synthesized and then cloned into pEG202 vector using Gateway LR Clonase II Enzyme Mix (Thermo Fisher Scientific). The original CaMV 35S promoter of pEG202 was substituted by the ubiquitin-10 promoter to drive the expression of AstD. The construct was electro-transformed into *Agrobacterium tumefaciens* strain Agl0 and then transformed into *A. thaliana* using the standard floral dip method[49]. The *A. thaliana* Col-0 ecotype was transformed. Positive transgenic plants were selected using the glufosinate resistance marker, and were tested for survival in the presence of aspterric acid.

Protein expression verification with western blot. Approximately 0.5 g of leaf tissue of transgenic *A. thaliana* was ground in liquid nitrogen. Proteins were homogenized in 2 × SDS buffer and then centrifuged at 21,000*g* for 5 min to remove undissolved debris. The supernatant containing resolved proteins were loaded onto a 4–12% Bis–Tris gel, and separated using MOPS running buffer. Transfer was conducted using an iBlot2 dry transfer device and a PVDF membrane. The total proteins were stained with Ponceau to demonstrate equal loading. Western blotting was performed using Sigma monoclonal anti-Flag M2-Peroxidase antibody, with detection using the Amersham ECL Prime detection reagent.

Reporting summary. Further information on experimental design is available in the Nature Research Reporting Summary linked to this paper.

Data availability. The data that support the findings of this study are available within the paper and its Supplementary Information, or are available from the corresponding authors upon reasonable request. The structural factor and coordinate of holo-*Ath*DHAD have been deposited in the Protein Data Bank under the ID 5ZE4.

31. Liu, N. et al. Identification and heterologous production of a benzoyl-primed tricarboxylic acid polyketide intermediate from the zaragozic acid A biosynthetic pathway. *Org. Lett.* **19**, 3560–3563 (2017).
32. Fang, F. et al. A vector set for systematic metabolic engineering in *Saccharomyces cerevisiae*. *Yeast* **28**, 123–136 (2011).
33. Cool, L. G. *ent*-Daucane and acorane sesquiterpenes from ×*Cupressocyparis leylandii* foliage. *Phytochemistry* **58**, 969–972 (2001).
34. Goldschmidt, L., Cooper, D. R., Derewenda, Z. S. & Eisenberg, D. Toward rational protein crystallization: a web server for the design of crystallizable protein variants. *Protein Sci.* **16**, 1569–1576 (2007).
35. Otwinowski, Z., Minor, W. & Jr, W. Processing of X-ray diffraction data collected in oscillation mode. *Methods Enzymol.* **276**, 307–326 (1997).
36. McCoy, A. J. et al. Phaser crystallographic software. *J. Appl. Crystallogr.* **40**, 658–674 (2007).
37. Winn, M. D. et al. Overview of the CCP4 suite and current developments. *Acta Crystallogr. D* **67**, 235–242 (2011).
38. Murshudov, G. N. et al. REFMAC5 for the refinement of macromolecular crystal structures. *Acta Crystallogr. D* **67**, 355–367 (2011).
39. Emsley, P., Lohkamp, B., Scott, W. G. & Cowtan, K. Features and development of Coot. *Acta Crystallogr. D* **66**, 486–501 (2010).
40. Harder, E. et al. OPLS3: a force field providing broad coverage of drug-like small molecules and proteins. *J. Chem. Theory Comput.* **12**, 281–296 (2016).
41. Søndergaard, C. R., Olsson, M. H. M., Rostkowski, M. & Jensen, J. H. Improved treatment of ligands and coupling effects in empirical calculation and rationalization of pKa values. *J. Chem. Theory Comput.* **7**, 2284–2295 (2011).
42. Eswar, N. et al. Comparative protein structure modeling using MODELLER. *Curr. Protoc. Bioinformatics* **47**, 5.6.1–5.6.32 (2006).
43. Greenwood, J. R., Calkins, D., Sullivan, A. P. & Shelley, J. C. Towards the comprehensive, rapid, and accurate prediction of the favorable tautomeric states of drug-like molecules in aqueous solution. *J. Comput. Aided Mol. Des.* **24**, 591–604 (2010).
44. Friesner, R. A. et al. Glide: a new approach for rapid, accurate docking and scoring. 1. Method and assessment of docking accuracy. *J. Med. Chem.* **47**, 1739–1749 (2004).
45. Yuan, S., Chan, H. C. S., Filipek, S. & Vogel, H. PyMOL and Inkscape bridge the data and the data visualization. *Structure* **24**, 2041–2042 (2016).
46. Yuan, S., Chan, H. C. S. & Hu, Z. Using PyMOL as a platform for computational drug design. *Wiley Interdiscip. Rev. Comput. Mol. Sci.* **7**, e1298 (2017).
47. Genheden, S. & Ryde, U. The MM/PBSA and MM/GBSA methods to estimate ligand-binding affinities. *Expert Opin. Drug Discov.* **10**, 449–461 (2015).
48. Sirin, S. et al. A computational approach to enzyme design: predicting ω-aminotransferase catalytic activity using docking and MM-GBSA scoring. *J. Chem. Inf. Model.* **54**, 2334–2346 (2014).
49. Clough, S. J. & Bent, A. F. Floral dip: a simplified method for *Agrobacterium*-mediated transformation of *Arabidopsis thaliana*. *Plant J.* **16**, 735–743 (1998).

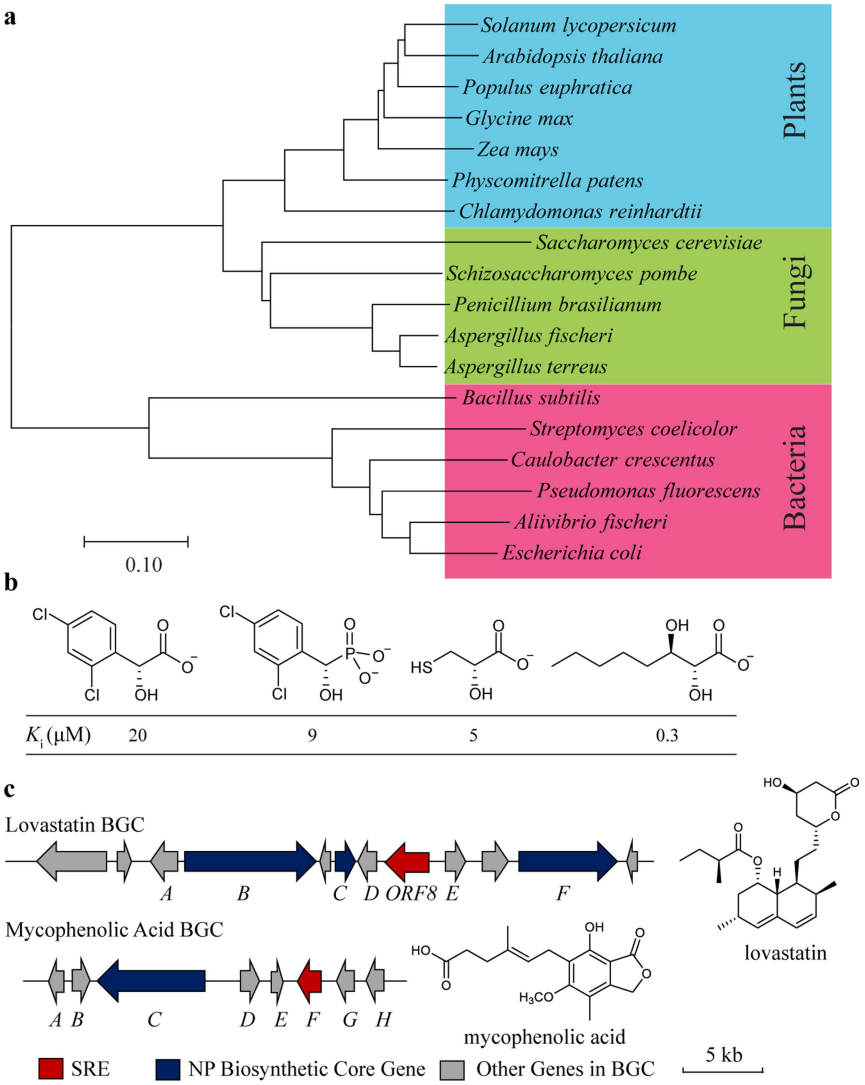

Extended Data Fig. 1 | The rationale of resistance-gene-directed discovery of a natural herbicide with a new mode of action. **a**, Phylogenetic tree of DHAD among bacteria, fungi and plants. The evolutionary history was inferred by using the neighbour-joining method (MEGA7). Scale-bar units represent the number of amino acid substitutions per site. **b**, Representatives of small molecules that inhibit DHAD in vitro, but fail to inhibit plant growth. **c**, Examples of co-localization of biosynthetic gene clusters (BGCs) and targets. The biosynthetic core genes are shown in blue and the self-resistance enzymes (SREs) are shown in red. The blockbuster cholesterol-lowering lovastatin drug targets HMG-CoA reductase (HMGR) in eukaryotes. In the fungus *A. terreus* that produces lovastatin, a second copy of HMGR encoded by ORF8 is present in the gene cluster (top). The BGC of the immunosuppressant mycophenolic acid from *Penicillium* sp. contains a second copy of inosine monophosphate dehydrogenase (IMPDH), which represents the SRE to this cluster (bottom).

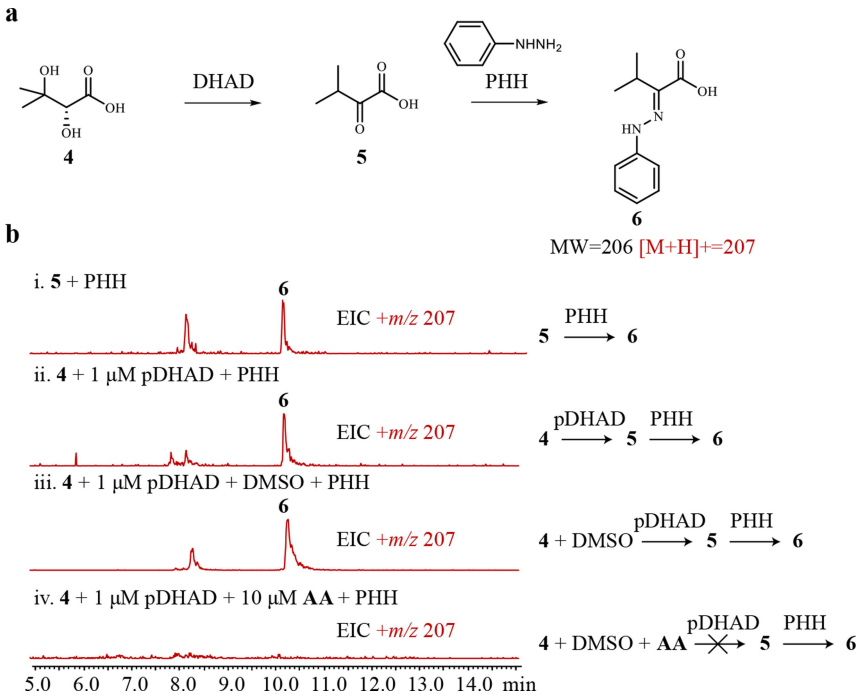

Extended Data Fig. 2 | Biochemical assays of DHAD functions. **a**, Assaying DHAD activities in the conversion of the dihydroxyacid **4** into the α-ketoacid **5**. Formation of **5** can be detected with HPLC by chemical derivatization using phenylhydrazine (PHH) to yield **6**. **b**, LC–MS traces of the biochemical assays of *Ath*DHAD (plant DHAD, pDHAD). EIC of positive ion mass of $[M + H]^+ = 207$ is shown in red. Panels i–iv in **b**: i, the derivatization reaction was validated by using the authentic **5**; ii, the bioactivity of *Ath*DHAD in converting **4** into **5** was validated; iii, addition of DMSO to *Ath*DHAD enzymatic reaction mixture has no effect; and iv, addition of 10 μM aspterric acid to the reaction mixture abolished *Ath*DHAD activity. The experiments were repeated independently three times with similar results.

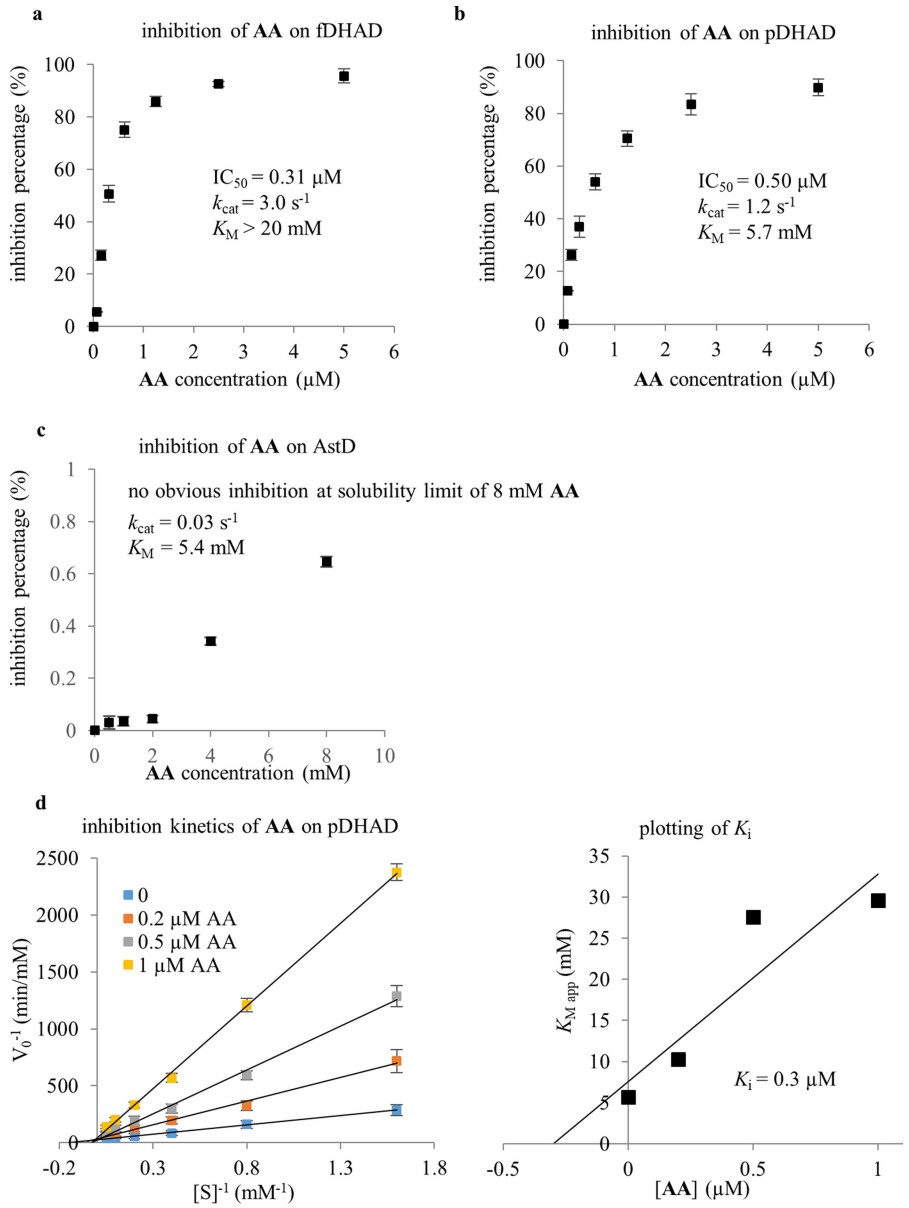

Extended Data Fig. 3 | Inhibition assay of different DHADs using aspterric acid. a–c, Three DHAD enzymes were assayed, including *Ath*DHAD (plant DHAD, pDHAD), *Ate*DHAD (fungal housekeeping DHAD from *A. terreus*, fDHAD) and AstD (DHAD homologue within *ast* cluster). IC_{50} and K_i values of aspterric acid were measured on the basis of inhibition percentage at different aspterric acid concentrations. Data are mean ± s.d. from three biologically independent experiments. **a**, Plot of the inhibition percentage of 0.5 μM *Ate*DHAD as a function of aspterric acid concentration. **b**, Plot of the inhibition percentage of 0.5 μM *Ath*DHAD as a function of aspterric acid concentration. **c**, Plot of the inhibition percentage of 0.5 μM AstD as a function of aspterric acid concentration. **d**, Analysis of inhibitory kinetics of aspterric acid on *Ath*DHAD using the Lineweaver–Burk method at different concentrations of aspterric acid (left). Linear fitting of the apparent Michaelis constant ($K_{M,app}$) as a function of aspterric acid concentration yields the K_i of aspterric acid on *Ath*DHAD (right).

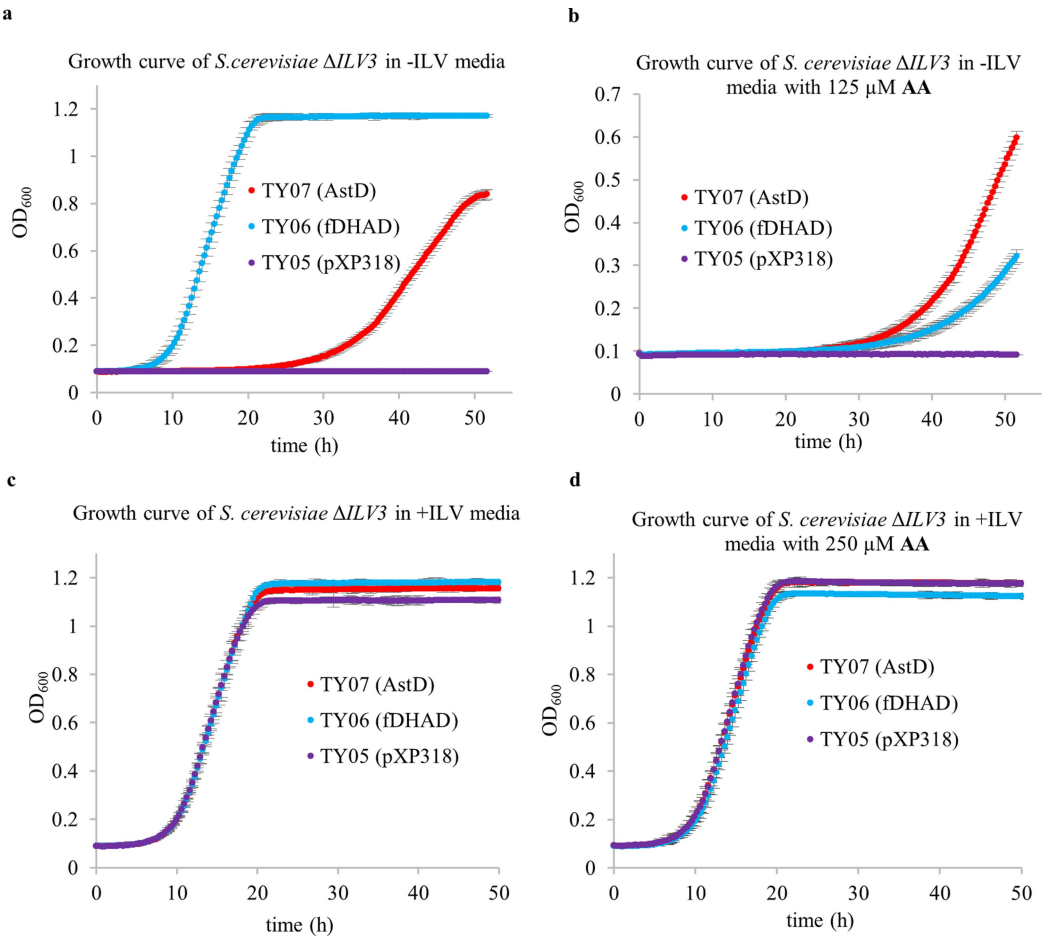

Extended Data Fig. 4 | Growth curve of *S. cerevisiae* Δ*ILV3* expressing AstD and *Ate*DHAD. a–d, The genome copy of DHAD encoded by *ILV3* was first deleted from *S. cerevisiae* strain DHY Δ*URA3* to give UB02. UB02 was then either chemically complemented by growth on ILV (leucine, isoleucine and valine)-containing medium or genetically by expressing of *Ate*DHAD (fungal housekeeping DHAD from *A. terreus*, fDHAD) or AstD episomally (TY06 or TY07, respectively). The empty vector pXP318 was also transformed into UB02 to generate a control strain TY05. Cell growth (optical density) under different conditions was plotted as a function of time. Data are mean ± s.d. from three biologically independent experiments. **a**, Growth curve in ILV dropout medium with no aspterric acid. **b**, Growth curve in ILV dropout medium with 125 μM aspterric acid. **c**, Growth curve in ILV supplemented medium. **d**, Growth curve in ILV supplemented medium with 250 μM aspterric acid.

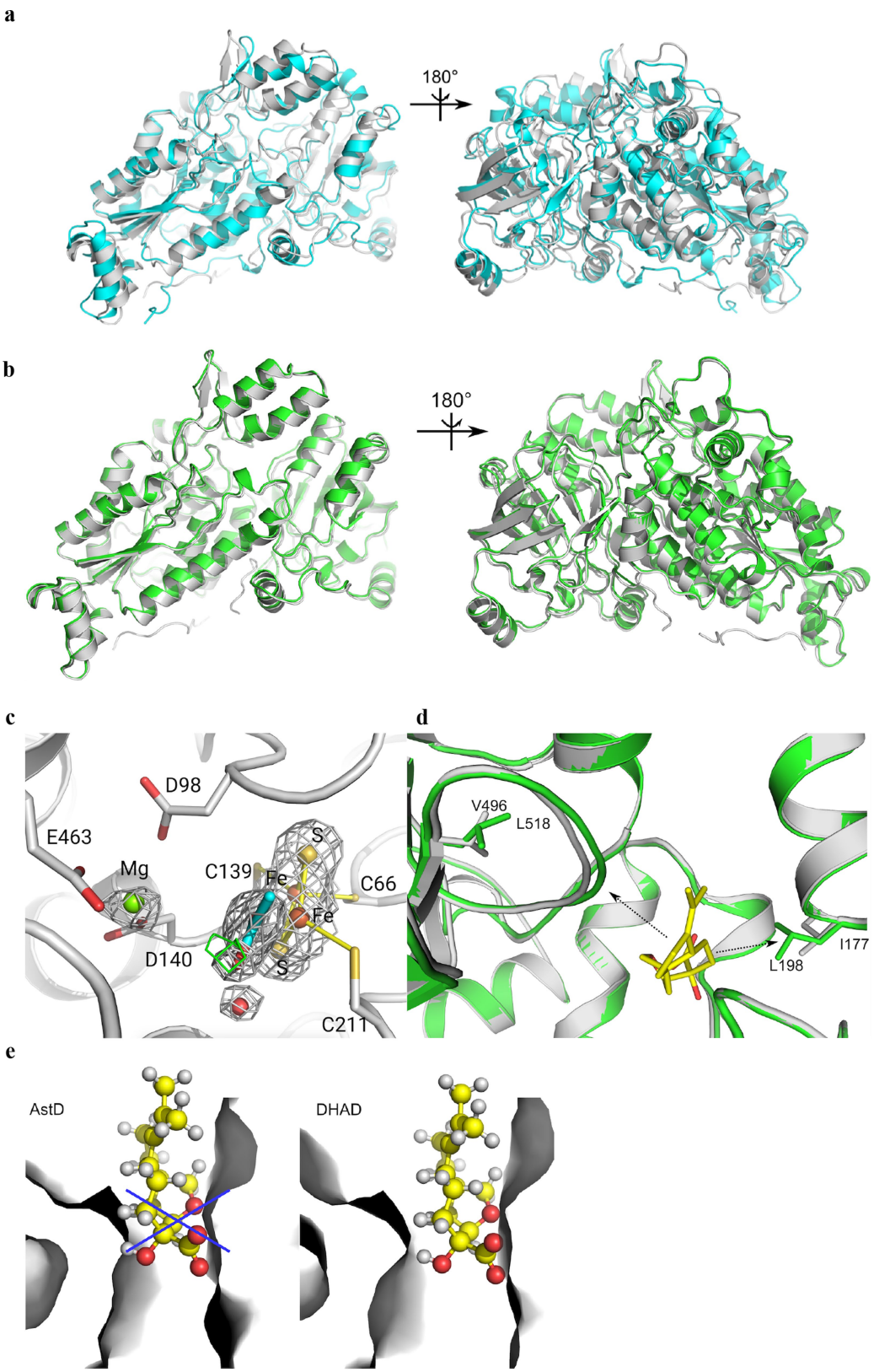

Extended Data Fig. 5 | See next page for caption.

Extended Data Fig. 5 | X-ray structure of holo-*Ath*DHAD and homology model of AstD. a, Superimpositions of the monomer of holo-*Ath*DHAD (PDB: 5ZE4, 2.11 Å) and RlArDHT (PDB: 5J84). The holo structure containing the 2Fe–2S cofactor and Mg^{2+} ion in the active site. The structure of holo-*Ath*DHAD is in white; the crystal structure of RlArDHT is in cyan. **b**, Superimpositions of holo-*Ath*DHAD and homology-modelled AstD. The structure of AstD was constructed by homology modelling on the basis of the structure of holo-*Ath*DHAD. The structure of holo-*Ath*DHAD is in white; the crystal structure of AstD is in green. **c**, The electron density map of cofactors in the holo structure of *Ath*DHAD. White mesh indicates the $2F_o - F_c$ map at the 1.2σ level; green mesh indicates the $F_o - F_c$ positive map at the 3.2σ level; cyan sticks represent the acetic acid molecule. **d**, Comparison of the active sites in the crystal structure of *Ath*DHAD and the modelled structure of AstD. The cartoon represents superimposed binding sites of *Ath*DHAD (white) and AstD (green). The shift of a loop in AstD, where L518 (corresponding to V496 in *Ath*DHAD) is located, coupled with a larger L198 residue (corresponding to I177 in *Ath*DHAD) leads to a smaller hydrophobic pocket in AstD than in *Ath*DHAD. **e**, The surface of binding sites of AstD (left) and *Ath*DHAD (right). The smaller hydrophobic channel in the modelled AstD cannot accommodate the aspterric acid molecule (yellow ball and stick model).

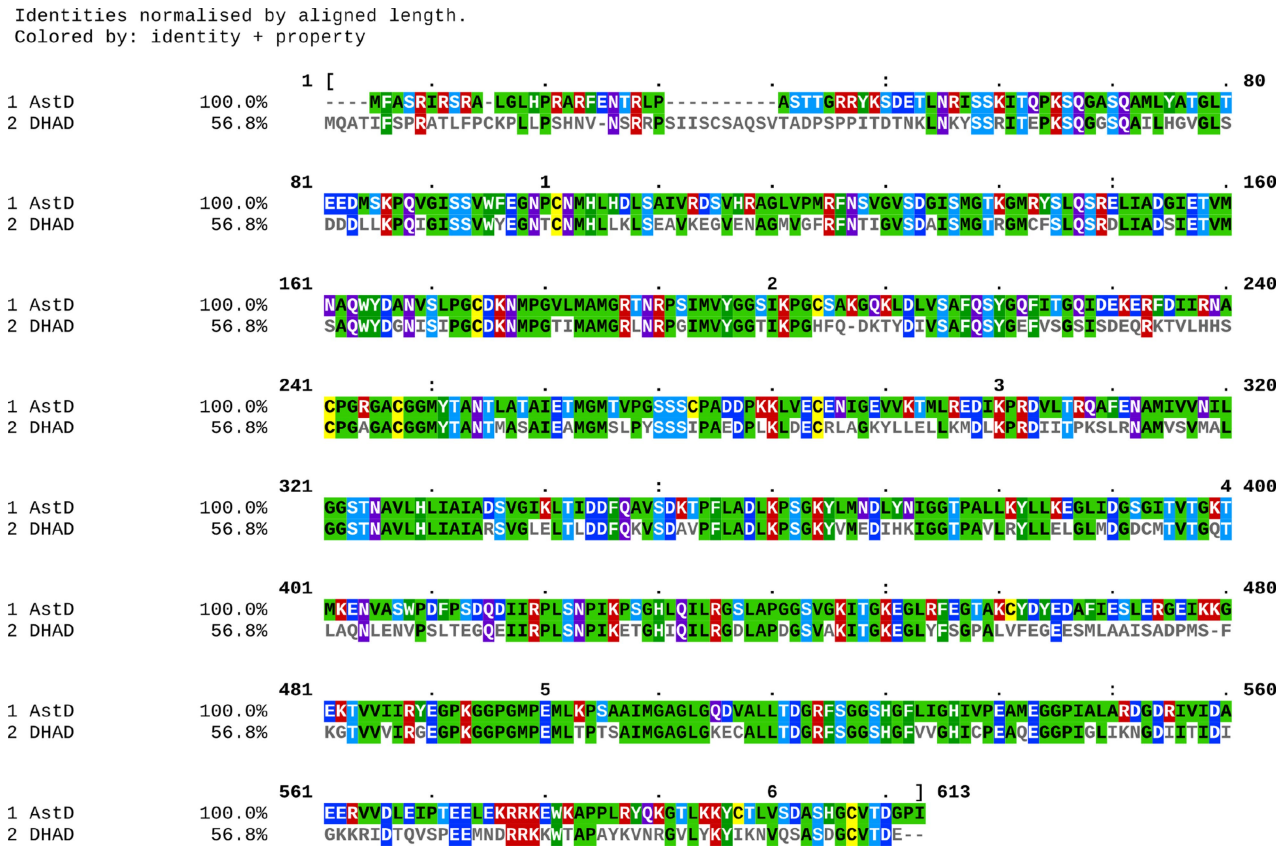

Extended Data Fig. 6 | Sequence alignment between *Ath*DHAD and AstD. The sequence identity between *Ath*DHAD and AstD is 56.8%, whereas the similarity between them is 75.0%. Residues were coloured according to their property and similarity.

Solvent 250 μM **AA** in solvent

Extended Data Fig. 7 | Spray assay of aspterric acid on *A. thaliana*. Glufosinate-resistant *A. thaliana* was treated with (right) or without (left) aspterric acid in the solvent, which is a commercial glufosinate-based herbicide marketed as Finale. To improve the wetting and penetration, aspterric acid was first dissolved in ethanol and then added to the solvent (0.06 g l^{-1} Finale (Bayer) with 20 g l^{-1} ethanol) to make 250 μM aspterric acid spraying solution. The control plants were treated with solvent containing ethanol only. Spraying treatments began upon seed germination, and were repeated once every two days with approximately 0.4 ml aspterric acid solution per time per pot for four weeks. The picture shown is taken after one month of treatment. The application rate of aspterric acid is approximately 1.6 lb per acre, which is comparable to the commonly used herbicide glyphosate (0.75–1.5 lb per acre). The experiments were repeated independently three times with similar results.

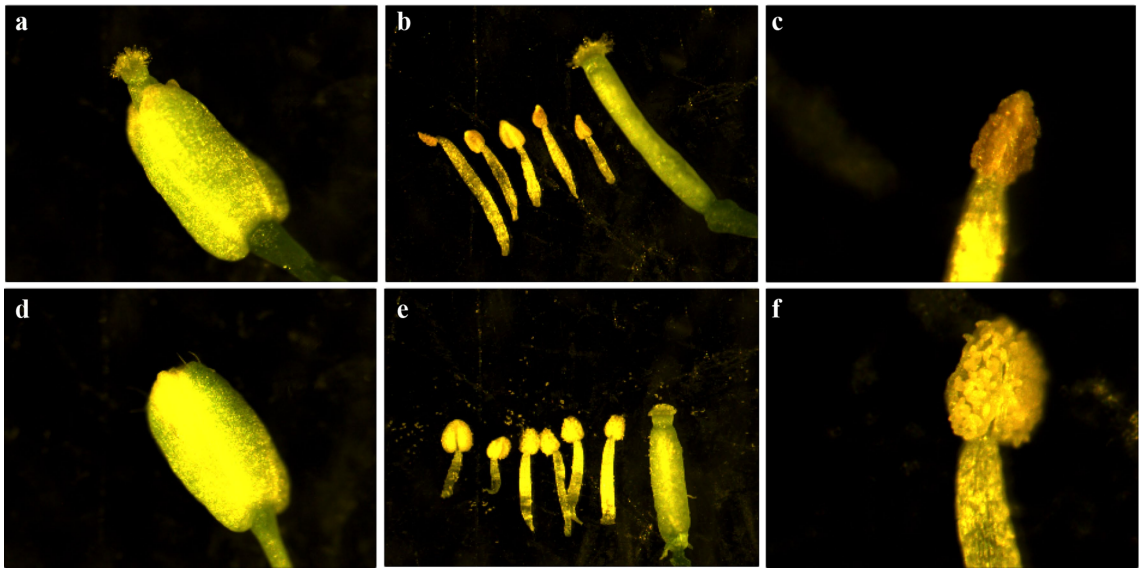

Extended Data Fig. 8 | Specific inhibition of anther development in *A. thaliana*. **a**–**f**, Comparison of flower organs between the aspterric acid-treated (**a**–**c**) and non-treated (**d**–**f**) *Arabidopsis*. **a**, **d**, The aspterric acid-treated flower shows abnormal pistil elongation owing to the lack of pollination. **b**, **e**, The aspterric acid treated flower is missing one stamen. **c**, **f**, The aspterric acid treated anther is depleted of healthy and mature pollen. The experiments were performed twice with similar results.

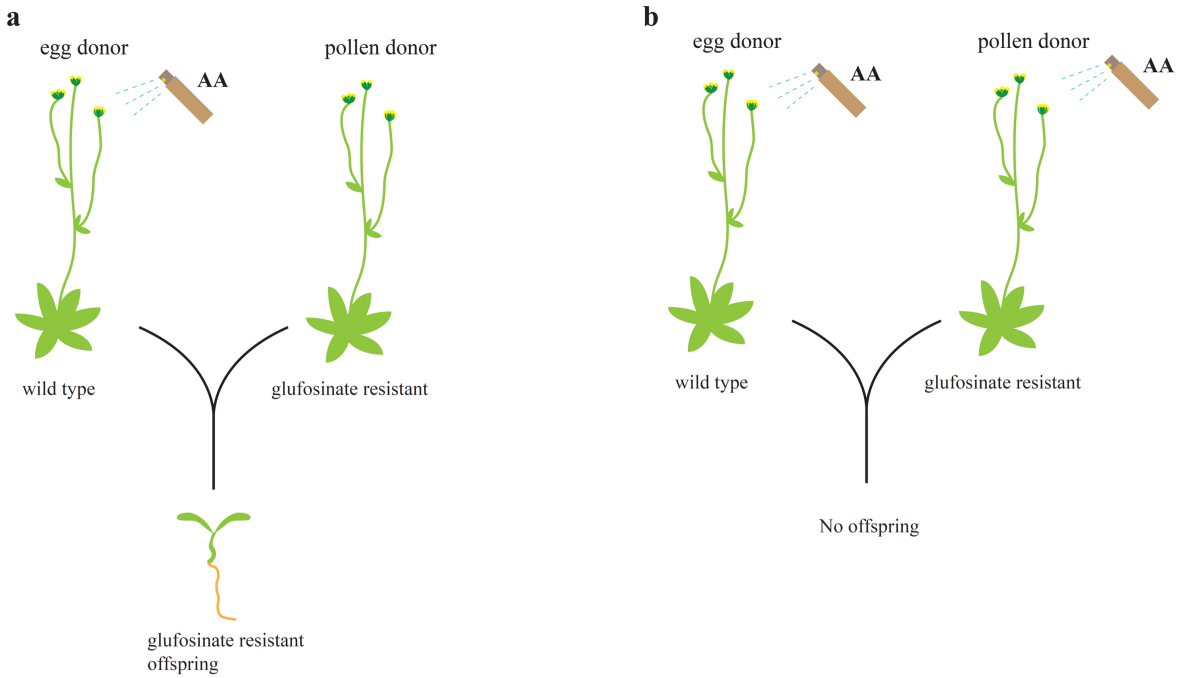

female parent	male parent	offspring obtained	inherit resistance
AA treated wild type	un-treated Glufosinate resistant plant	Yes	Yes
AA treated wild type	**AA** treated glufosinate resistant plant	No	N/A

Extended Data Fig. 9 | Schematic of results from the cross experiment. **a**, Wild-type *A. thaliana* treated with 250 μM aspterric acid was pollinated with pollen from the un-treated plant that carries the glufosinate-resistance gene. Offspring was obtained, and inherited the glufosinate resistance from the pollen donor. **b**, As in **a**, except that the pollen donor was also treated with 250 μM aspterric acid. No offspring was obtained from this cross. Similar results were obtained after treatment with 100 μM aspterric acid.

Extended Data Table 1 | Data collection and refinement statistics (molecular replacement)

	holo-*Ath*DHAD
Data collection	
Space group	$P4_22_12$
Cell dimensions	
a, *b*, *c* (Å)	135.5, 135.5, 66.0
α, β, γ (°)	90, 90, 90
Resolution (Å)	47.89-2.11 (2.15-2.11) *
R_{sym} or R_{merge}	0.189 (1.240)
I / σI	17.86 (2.33)
Completeness (%)	100 (100)
Redundancy	25.1 (23.1)
Refinement	
Resolution (Å)	30.00-2.11
No. reflections	33076 (1709)
R_{work} / R_{free}	0.1727 / 0.2152
No. atoms	
Protein	4224
Ligand/ion	24
Water	118
B-factors	
Protein	26.60
Ligand/ion	46.53
Water	26.22
R.m.s. deviations	
Bond lengths (Å)	0.007
Bond angles (°)	1.191

*Values in parentheses are for the highest-resolution shell.

nature research

Corresponding author(s): Yi Tang

Reporting Summary

Nature Research wishes to improve the reproducibility of the work that we publish. This form provides structure for consistency and transparency in reporting. For further information on Nature Research policies, see Authors & Referees and the Editorial Policy Checklist.

Statistical parameters

When statistical analyses are reported, confirm that the following items are present in the relevant location (e.g. figure legend, table legend, main text, or Methods section).

n/a	Confirmed	
☐	☒	The exact sample size (*n*) for each experimental group/condition, given as a discrete number and unit of measurement
☐	☒	An indication of whether measurements were taken from distinct samples or whether the same sample was measured repeatedly
☒	☐	The statistical test(s) used AND whether they are one- or two-sided *Only common tests should be described solely by name; describe more complex techniques in the Methods section.*
☒	☐	A description of all covariates tested
☒	☐	A description of any assumptions or corrections, such as tests of normality and adjustment for multiple comparisons
☐	☒	A full description of the statistics including central tendency (e.g. means) or other basic estimates (e.g. regression coefficient) AND variation (e.g. standard deviation) or associated estimates of uncertainty (e.g. confidence intervals)
☒	☐	For null hypothesis testing, the test statistic (e.g. *F*, *t*, *r*) with confidence intervals, effect sizes, degrees of freedom and *P* value noted *Give P values as exact values whenever suitable.*
☒	☐	For Bayesian analysis, information on the choice of priors and Markov chain Monte Carlo settings
☒	☐	For hierarchical and complex designs, identification of the appropriate level for tests and full reporting of outcomes
☒	☐	Estimates of effect sizes (e.g. Cohen's *d*, Pearson's *r*), indicating how they were calculated
☐	☒	Clearly defined error bars *State explicitly what error bars represent (e.g. SD, SE, CI)*

Our web collection on statistics for biologists may be useful.

Software and code

Policy information about availability of computer code

Data collection	Diffraction data of holo-pDHAD was indexed, integrated, and scaled using the HKL3000 package.
Data analysis	The phylogenetic analysis was done by using MEGA (Molecular Evolutionary Genetics Analysis) version 7. The holo-pDHAD structure was solved by the molecular replacement method Phaser embedded in the CCP4i suite, the resulting model were refined against the diffraction data using the REFMAC5 program of CCP4i. The side chains of holo-pDHAD protein, iron sulfur cluster, water molecule, acetate ion, sulfate ions, and magnesium ion were manually built using the program WinCoot. The geometry of the model was validated by WinCoot. Homology modeling of AstD and docking of substrates to holo-pDHAD was performed using Schrodinger suite software and Glide respectively. Hydrogen atoms were added to crystal structures with the PROPKA tool in Protein Preparation tool in Maestro to optimize the hydrogen bond network. The homology model was performed in Modeller 9.18. The ionization state of ligands were calculated with Epik tool employing Hammett and Taft methods in conjunction with ionization and

tautomerization tools. Figures are prepared in PyMOL and Inkscape.

The MM/GBSA calculations had been done in Prime (Schrödinger 2015 suite). Protein–ligand van der Waals contacts, electrostatic interactions, ligand desolvation, and internal strain energies, using VSGB2.0 implicit solvent model with the OPLS2005 force field.

For manuscripts utilizing custom algorithms or software that are central to the research but not yet described in published literature, software must be made available to editors/reviewers upon request. We strongly encourage code deposition in a community repository (e.g. GitHub). See the Nature Research guidelines for submitting code & software for further information.

Data

Policy information about availability of data

All manuscripts must include a data availability statement. This statement should provide the following information, where applicable:

- Accession codes, unique identifiers, or web links for publicly available datasets
- A list of figures that have associated raw data
- A description of any restrictions on data availability

All the data supporting this report is available in maintext and supplementary information.

Field-specific reporting

Please select the best fit for your research. If you are not sure, read the appropriate sections before making your selection.

☒ Life sciences ☐ Behavioural & social sciences

For a reference copy of the document with all sections, see nature.com/authors/policies/ReportingSummary-flat.pdf

Life sciences

Study design

All studies must disclose on these points even when the disclosure is negative.

Sample size	The sample size of Arabidopsis plants was determined based on two factors 1. sufficient amount of plants are included to determine the consistence ; 2. Individual plants are properly spaced to allowed accurate measuring of their phenotype. Our Arabidopsis sample size (n) is always bigger than 10. The phenotype of plants that are growing on media is highly consistent, with minimal variation.
Data exclusions	no data was excluded.
Replication	Multiple transgenic plants were examined. The experiments were repeated on different days. We also tested different generations of the transgenic plants, to make sure the phenotype is consistent and stable. All attempts at replication were successful.
Randomization	Plants of different genetic backgrounds were randomly positioned to mitigate potential variables, which include the availability of water, light and air flow.
Blinding	Data collection, such as the measurements of weight and height were conducted by a third person who was blinded to sample identities.

Materials & experimental systems

Policy information about availability of materials

n/a	Involved in the study
☒	☐ Unique materials
☐	☒ Antibodies
☐	☒ Eukaryotic cell lines
☒	☐ Research animals
☒	☐ Human research participants

Antibodies

Antibodies used	Sigma-Aldrich A8592, monoclonal anti-FLAG M2-Peroxidase antibody. ~1mg/ml, 1:20000
Validation	the validation is on manufacturer's website (https://www.sigmaaldrich.com/). The following citation suggests that this antibody is suitable for detecting FLAG-tagged protein in Arabidopsis. (Saucet SB, Ma Y, Sarris PF, et al. Nature Communication, 6(6), 2015)

Eukaryotic cell lines

Policy information about cell lines

Cell line source(s)	melanoma cell line A375 and SK-MEL-1 was purchased from ATCC®
Authentication	none of the cell lines used were authenticated.
Mycoplasma contamination	cell lines were not tested for mycoplasma contamination
Commonly misidentified lines (See ICLAC register)	*Name any commonly misidentified cell lines used in the study and provide a rationale for their use.*

Method-specific reporting

n/a	Involved in the study
☒	☐ ChIP-seq
☒	☐ Flow cytometry
☒	☐ Magnetic resonance imaging